actuators

MDPI

*Article*

# Design and Implementation of an $\mathcal{L}_1$ Adaptive Proportional Output Feedback Controller

**Deepanshu Bagati, Toufik Souanef and James F. Whidborne ***

School of Aerospace Transport and Manufacturing, Cranfield University, Bedford MK43 0AL, UK; deepanshubagati64@gmail.com (D.B.); toufik.souanef@cranfield.ac.uk (T.S.)
* Correspondence: j.f.whidborne@cranfield.ac.uk

**Abstract:** A new approach for output feedback $\mathcal{L}_1$ adaptive control based on a proportional adaptation law is presented. The effectiveness of this design is assessed in simulation and validated through real-time testing on an airfoil pitch control wind tunnel experimental rig. Experimental evaluation of the robustness of the controllers, assessed by introducing various disturbances into the control signals, shows that the adaptive control has a better performance compared to PID control, particularly in scenarios with reduced control effectiveness and time-varying disturbances. The experimental results demonstrate the efficacy of the proposed method in practical applications.

**Keywords:** $\mathcal{L}_1$ adaptive control; fault-tolerant control; output feedback control; real-time systems

## 1. Introduction

Control systems have played a crucial role in aerospace, employing a variety of methods to enhance performance and ensure the resilience of aerospace systems [1]. Traditional controllers were designed to handle small perturbations about a particular operating point, and if there were uncertainties or large variations present, the system could become unstable or perform poorly. As a result, the concept of adaptive control theory was introduced, which involved modifying controller parameters in response to unknown plant variations [2].

One commonly used approach is model reference adaptive control (MRAC); this calculates the controller parameters in order to make an unknown dynamic system follow the desired reference model behaviour [3]. There are two ways to put this into action: direct and indirect [2]. In the indirect approach, the first step involves estimating the parameters of the plant. Once these parameters are known, they are used to compute the appropriate controller parameters. The direct approach, on the other hand, involves directly determining the controller gains needed to achieve the desired system behaviour.

From MRAC systems analysis, it is straightforward to show that improving the response to system variations can be achieved with high adaptation gains [4]. However, it was identified that doing so would lead to a reduction in the time-delay margin and the introduction of high-frequency oscillations in the control signal [4]. Furthermore, the absence of proper guidelines for determining an adequate adaptation rate means a greater dependence on extensive simulations or trial-and-error methods. The challenge was to select the right adaptation gain and ensure good performance bounds in transient regime. Hence, $\mathcal{L}_1$ adaptive control architecture was developed to decouple the adaptation rate from the system robustness [5]. $\mathcal{L}_1$ adaptive control includes a low-pass filter in the control channel, thus limiting its bandwidth. Inclusion of the low-pass filter helps compensate for the uncertainty within the bandwidth of control channel.

$\mathcal{L}_1$ adaptive control has been applied for various practical control systems—[6–13], to cite a few. However, relatively few methods have been presented for output feedback $\mathcal{L}_1$ adaptive control. The first approach employed a projection-based adaptive law [14],

check for updates

**Citation:** Bagati, D.; Souanef, T.; Whidborne, J.F. Design and Implementation of an $\mathcal{L}_1$ Adaptive Proportional Output Feedback Controller. *Actuators* **2024**, *13*, 172. https://doi.org/10.3390/act13050172

Academic Editor: Ioan Ursu

Received: 28 March 2024
Revised: 27 April 2024
Accepted: 30 April 2024
Published: 2 May 2024

but was constrained to first-order reference systems. Another option, applied to some aerospace problems, caters to non-strictly positive real reference systems [15], utilising a piecewise-adaptive law to meet desired performance bounds. In [16], an $\mathcal{L}_1$ adaptive output feedback controller was applied to manage disturbances at the system output, successfully demonstrated in managed pressure drilling experiments. Similarly, Lee et al [17] devised an $\mathcal{L}_1$ adaptive output feedback controller for underactuated multi-input–multi-output (MIMO) systems, augmenting an existing three-loop autopilot. This methodology found application in temperature control, as detailed in [18], while Ma and Cao [19] showcased its integration with model predictive control for multivariable nonlinear systems subject to constraints. Additionally, Ma and Cao [20] explored the application of $\mathcal{L}_1$ adaptive output feedback control to general partial differential equation (PDE) systems, and Zhou et al [21] addressed uncertain nonlinear systems with unmodelled dynamics and actuator faults utilising a similar design strategy. The primary limitation of these approaches lies in their reliance on transfer function formulation, which makes the interpretation of uncertainties and reference models less intuitive compared to a state-space model formulation [22,23]. Indeed, state variables offer a more comprehensive reflection of the internal characteristics of a system [21,24]. However, the main limitation of the approach presented in [22,24] is that it is restricted to non-minimum phase systems with a relative degree of one.

Furthermore, although $\mathcal{L}_1$ adaptive control has been successfully demonstrated in various applications in simulation environments, its practical implementations in real aerospace systems are few.

However, several devices have been created for the purpose of demonstrating the working of feedback control on experimental laboratory rigs. For example, Mansor et al [25] conducted an experiment to test the performance of a standard PID control algorithm using the 3-DOF helicopter rig from [26]. Subramanian et al [27] implemented model reference adaptive control on a 2-DOF helicopter rig from [28] by incorporating a baseline LQR controller. They were able to improve the stability characteristics by achieving faster convergence. For fixed-wing aircraft, Villarreal-Valderrama et al [29] built a wind tunnel test bed to study aircraft pitch control. They tested a PID controller and a loop shaping compensator on the test bed and found that both produced responses that were similar to the theoretical response. This demonstrated the suitability of their test unit for teaching or educational purposes. This is similar to the flight control demonstrator unit used in this paper [30,31], which was designed to as a demonstrator of some of the principles of automatic flight control. The equipment consists of a basic aerofoil in a wind tunnel, as shown in the schematic in Figure 1. The aerofoil is a NACA 0012 and is free to pitch about a horizontal axis located at the centre of gravity. It is controlled by an elevator that is driven by a servomotor controlled by an Arduino board that receives the pivot axis angle measurement from a potentiometer.

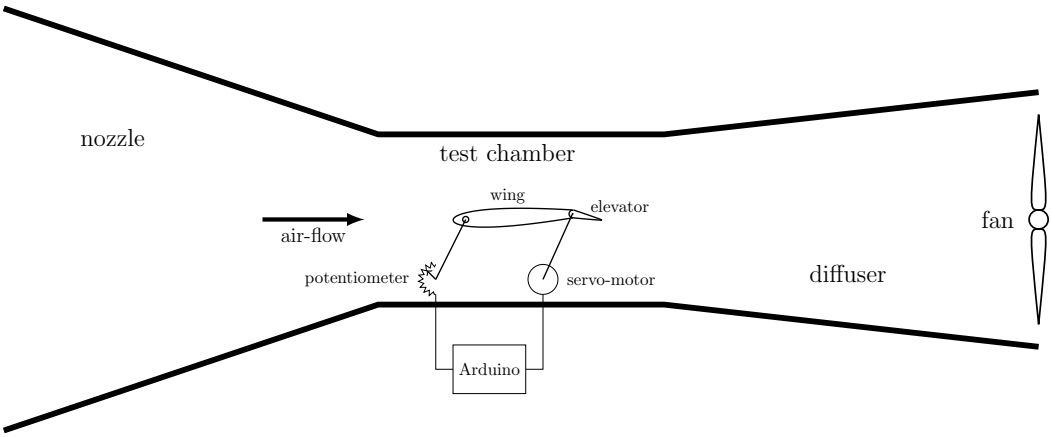


**Figure 1.** Flight control demonstrator unit—aerofoil in a wind tunnel.

This paper demonstrates the real-world applicability of an output feedback $\mathcal{L}_1$ adaptive control approach via its implementation on the automatic flight control demonstrator unit. The approach is based on the proportional adaptation law that directly relates the adaptation to the estimate error [32]. This method reduces computational processing time by making the error bounds proportional to the adaptation gain, in contrast to the gradient descent approach where the relation is with the square root of the adaptation gain. Additionally, this architecture introduces phase margin in the estimation loop, enabling the state predictor to incorporate first-order sensor dynamics. Although the initial approach relies on complete state feedback, here it is extended to the output feedback control case. Another advantage of using this approach is that it can be applied to non-semi-positive real (SPR) systems, i.e., it relaxes the assumption of non-minimum phase systems with a relative degree of one [22,24] while maintaining the state-space formulation of the systems.

The remainder of this paper is organised as follows. Section 2 describes the proportional $\mathcal{L}_1$ adaptive controller design. In Section 3, the analysis of the $\mathcal{L}_1$ adaptive control is presented. Simulation results are presented in Section 4. In Section 5, the implementation of the designed controller for the airfoil system is discussed. Finally, some conclusions are drawn.

## 2. Output Feedback Proportional $\mathcal{L}_1$ Adaptive Controller

In this section, the theory and design of the output feedback proportional adaptive law are provided. The design mostly builds upon the original proportional adaptive law introduced by Vanness et al [32,33]. The significant change made is to the adaptation law itself. As a result, the overall structure and analysis remain quite similar. The proofs have been recreated, with the main difference appearing in how the estimation error is bounded.

*Problem Formulation*

The controlled system (plant) dynamics are represented in a state space form:

$$\begin{aligned} \dot{x}(t) &= A_m x(t) + B_m \omega u(t) + f(t, x(t)) \\ y(t) &= C^\top x(t), \quad x(0) = x_0, \end{aligned} \tag{1}$$

where $x(t)$ is the plant state vector, $u(t)$ is the control signal, $B_m$ is a known constant vector, $A_m$ is a known Hurwitz matrix representing the desired model dynamics, $\omega$ is unknown input gain and $f$ is an unknown continuous nonlinear map representing uncertainties. The control objective is to design an output feedback controller such that the output $y(t)$ tracks a bounded continuous reference input $r(t)$.

**Assumption 1.** *The given control design assumes that there exists positive constants, denoted as L and B, such that*

$$\begin{aligned} \|f(t, x_1) - f(t, x_2)\|_\infty &\leq L\|x_1 - x_2\|_\infty \\ \|f(t, x)\|_\infty &\leq L\|x\|_\infty + B \end{aligned}$$

*where the numbers L and B can be arbitrarily large.*

**Assumption 2.** *The unknown input gain $\omega$ is bounded, i.e., $0 < \omega_l \leq \omega \leq \omega_u$.*

Control Architecture

The proposed control design involves a state predictor, an adaptation law and a control law, as shown in Figure 2.

State Predictor: Consider the following state predictor:

$$\begin{aligned} \dot{\hat{x}}(t) &= A_m \hat{x}(t) + B_m \omega_0 u(t) + \hat{\eta}(t), \quad \hat{x}(0) = x_0 \\ \hat{y}(t) &= C^\top \hat{x}(t), \end{aligned} \tag{2}$$

where $\omega_0$ is the appropriate guess for unknown input gain $\omega$, and overall uncertainties are then combined together to form the vector of estimates $\hat{\eta}(t)$.

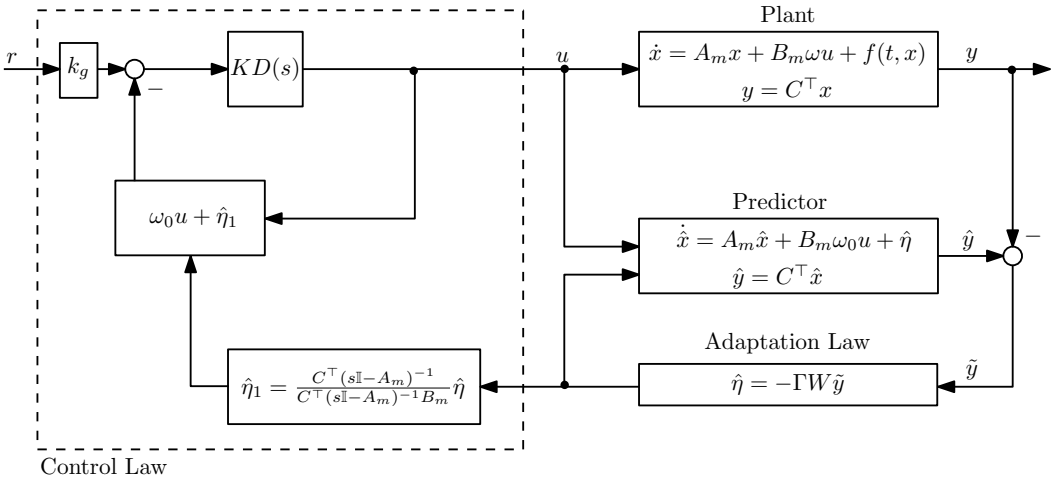


**Figure 2.** $\mathcal{L}_1$ adaptive control architecture (proportional).

Adaptation Law: The proposed adaptation law extends the state feedback case [32,33] to output feedback. The adaptation is determined by

$$\hat{\eta}(t) = -\Gamma W \tilde{y}(t) \tag{3}$$

where $\tilde{y}(t) = \hat{y}(t) - y(t)$ is the output prediction error, $\Gamma$ is the adaptation gain and $W$ is a $n \times m$ arbitrary matrix such that $WC^\top \neq 0$.

Control Law: The control law is defined by

$$\begin{aligned} u(s) &= -KD(s)(\omega_0 u(s) + \hat{\eta}_1(s) - k_g r(s)), \\ \hat{\eta}_1(s) &= \phi(s)\hat{\eta}(s), \;\; \phi(s) = \frac{C^\top (s\mathbb{I} - A_m)^{-1}}{C^\top (s\mathbb{I} - A_m)^{-1} B_m}, \end{aligned} \tag{4}$$

where $r(s)$ and $\hat{\eta}(s)$ are the frequency domain representations of $r(t)$ and $\hat{\eta}(t)$, respectively; $k_g = 1/(C^\top A_m^{-1} B_m)$ is the feedforward gain meant to eliminate steady-state error; $D(s)$ is a strictly proper transfer function; and $K$ is the feedback gain, which gives

$$C(s) = \frac{\omega k D(s)}{1 + \omega k D(s)}$$

which is a strictly proper transfer function with a steady-state gain $C(0) = 1$. The above described controller is subjected to the following $\mathcal{L}_1$-norm condition:

$$\|G(s)\|_{\mathcal{L}_1} L < 1$$

where

$$\begin{aligned} &G(s) = (\mathbb{I}_n - H_{xm}(s) C(s) H_m^{-1}(s) C^\top) H_{xum}(s), \\ &H_{xum}(s) = (s\mathbb{I} - A_m)^{-1}, \; H_{xm}(s) = (s\mathbb{I} - A_m)^{-1} B_m, \\ &H_m(s) = C^\top (s\mathbb{I} - A_m)^{-1} B_m \end{aligned}$$

## 3. Controller Analysis

In this section, the performance of the $\mathcal{L}_1$ adaptive controller is analysed. More specifically, the following are shown:

- The reference model resulting from perfect knowledge of the uncertainties and a corresponding non-adaptive controller is stable, subject to some conditions involving the filter.
- The prediction error, i.e., the error between the state of the plant and that of the state predictors, is bounded.
- The difference between the state/input of the system and those of the reference system is proportional to the prediction error.

### *3.1. Reference System Analysis*

Consider the following closed-loop reference system:

$$\begin{aligned} \dot{x}_{\text{ref}}(t) &= A_m x_{\text{ref}}(t) + B_m \omega u_{\text{ref}}(t) + \eta_{\text{ref}}(t), \;\; x_{\text{ref}}(0) = x_0 \\ y_{\text{ref}}(t) &= C^\top x_{\text{ref}}(t) \\ \eta_{\text{ref}}(t) &= f(t, x_{\text{ref}}(t)) \\ u_{\text{ref}}(s) &= -\frac{C(s)}{\omega}(\phi(s)\eta_{\text{ref}}(s) - k_g r(s)) \end{aligned} \tag{5}$$

**Lemma 1.** *If $K$ and $D(s)$ satisfy the $\mathcal{L}_1$-norm condition, then the closed-loop reference system is BIBS stable with respect to reference $r(t)$ and initial state vector $x_0$.*

**Proof.** It follows from (5) that

$$x_{\text{ref}}(s) = G(s)\eta_{\text{ref}}(s) + H_{xm}(s)C(s)k_g r(s) + x_{in}(s) \tag{6}$$

where $x_{in}(s) = (s\mathbb{I} - A_m)^{-1}x_0$ is bounded since $A_m$ is Hurwitz. Then, it follows that

$$\|x_{\text{ref}\tau}\|_{\mathcal{L}_\infty} \leq \|G(s)\|_{\mathcal{L}_1}\|\eta_{\text{ref}\tau}\|_{\mathcal{L}_\infty} + \|H_{xm}(s)C(s)k_g\|_{\mathcal{L}_1}\|r\|_{\mathcal{L}_\infty} + \|x_{in}\|_{\mathcal{L}_\infty} \tag{7}$$

and using Assumption 1, the upper bound for $\eta_{\text{ref}}(t)$ is

$$\|\eta_{\text{ref}\tau}\|_{\mathcal{L}_\infty} \leq L\|x_{\text{ref}\tau}\|_{\mathcal{L}_\infty} + B$$

Substituting and solving for $\|x_{\text{ref}\tau}\|_{\mathcal{L}_\infty}$,

$$\|x_{\text{ref}\tau}\|_{\mathcal{L}_\infty} \leq \frac{\|G(s)\|_{\mathcal{L}_1}B + \|H_{xm}(s)C(s)k_g\|_{\mathcal{L}_1}\|r\|_{\mathcal{L}_\infty} + \|x_{in}\|_{\mathcal{L}_\infty}}{1 - \|G(s)\|_{\mathcal{L}_1}L} \tag{8}$$

Hence, $\|x_{\text{ref}\tau}\|_{\mathcal{L}_\infty}$ is bounded if $K$ and $D(s)$ verify the $\mathcal{L}_1$-norm condition. □

### *3.2. Estimation Error Analysis*

The following lemma states that the bound of the state estimation error $\tilde{x}(t) = \hat{x}(t) - x(t)$ is uniformly bounded.

**Lemma 2.** *If the closed-loop system is stable, then the estimation error is uniformly bounded, and its bound is defined by*

$$\|\tilde{x}_\tau\|_{\mathcal{L}_\infty} \leq \gamma_0 = \frac{\Delta_m}{\Gamma\|WC\|}\left(\frac{\lambda_{max}(P)}{\lambda_{min}(P)}\right)^{3/2} \tag{9}$$

*where $\Delta_m$ is defined below.*

**Proof.** From (1) and (2), the prediction error can be written as

$$\begin{aligned} \dot{\tilde{x}}(t) &= A_m\tilde{x}(t) + \hat{\eta}(t) - \eta(t) + B_m(\omega_0 - \omega)u(t) \\ \tilde{y}(t) &= C^\top\tilde{x}(t), \;\; \tilde{x}(0) = \tilde{x}_0 = 0 \end{aligned} \tag{10}$$

Rewriting the prediction error dynamics in frequency domain, we have

$$C^\top \tilde{x}(s) = H_m(s)\tilde{\eta}(s)$$

where

$$\tilde{\eta}(s) = (\omega_0 - \omega)u(s) + \hat{\eta}_1(s) - \eta_1(s)$$

and $\eta_1(s) = \phi(s)\eta(s)$.

Now, we consider the Lyapunov function candidate

$$V(t) = \frac{1}{2\Gamma}\tilde{x}^\top(t)P\tilde{x}(t) \tag{11}$$

where $P$ is the solution of the Lyapunov equation

$$A_m^\top P + PA_m = -Q$$

where $Q = Q^\top > 0$ is an arbitrary positive definite matrix. Hence, including the adaptation law, it can be written

$$\begin{aligned}\dot{V}(t) = &-\frac{1}{2\Gamma}\tilde{x}^\top(t)Q\tilde{x}(t) - \tilde{x}^\top(t)PWC^\top\tilde{x}(t) \\ &+ \frac{1}{\Gamma}\tilde{x}^\top(t)P(B_m(\omega_0 - \omega)u(t) - \eta(t))\end{aligned} \tag{12}$$

Hence, an upper bound can be derived for $t \in [0, \tau]$

$$\dot{V}(t) \leq -\lambda_{min}(P)\|WC\|\|\tilde{x}(t)\|^2 + \frac{1}{\Gamma}\|\tilde{x}(t)\|\lambda_{max}(P)\Delta_m \tag{13}$$

where $\Delta_m$ is bounded as

$$\|B_m(\omega_0 - \omega)u(t) - \eta(t)\| \leq \Delta_m = (\omega_u - \omega_l)\|B_m\|\rho_u + \sqrt{n}(L\rho + B) \tag{14}$$

where $\rho$ and $\rho_u$ are the upper bounds for state and control variable, respectively. Hence,

$$\dot{V}(t) < 0 \text{ if } \|\tilde{x}(t)\| > \frac{\lambda_{max}(P)\Delta_m}{\lambda_{min}(P)\|WC\|\Gamma} \tag{15}$$

and since $\frac{1}{2\Gamma}\lambda_{min}(P)\|\tilde{x}(t)\|^2 \leq V(t)$, we obtain

$$\|\tilde{x}_\tau\|_{\mathcal{L}_\infty} \leq \frac{\Delta_m}{\Gamma\|WC\|}\left(\frac{\lambda_{max}(P)}{\lambda_{min}(P)}\right)^{3/2} \tag{16}$$

□

### *3.3. Performance Bounds Analysis*

In the following theorem, the performance bounds of $\mathcal{L}_1$ proportional adaptive law are shown.

**Theorem 1.** *Given the system* (1)*, the reference system* (5) *and the* $\mathcal{L}_1$ *adaptive controller* (2) *to* (4)*, we have*

$$\begin{aligned}\|x_{ref} - x\|_{\mathcal{L}_\infty} &\leq \gamma_1 \\ \|u_{ref} - u\|_{\mathcal{L}_\infty} &\leq \gamma_2\end{aligned} \tag{17}$$

*where*

$$\gamma_1 = \frac{\left\| H_{xm}(s)C(s)H_m^{-1}(s)C^\top \right\|_{\mathcal{L}_1}}{1 - \|G(s)\|_{\mathcal{L}_1} L}\gamma_0$$
$$\gamma_2 = \left\| \frac{C(s)}{\omega}\phi(s) \right\|_{\mathcal{L}_1} L\gamma_1 + \left\| \frac{C(s)H_m^{-1}(s)C^\top}{\omega} \right\|_{\mathcal{L}_1} \gamma_0$$

**Proof.** The control law (4) can be written as

$$u(s) = -\frac{C(s)}{\omega}(\eta_1(s) + \tilde{\eta}(s) - k_g r(s)) \tag{18}$$

Converting the plant dynamics to frequency domain and substituting the given control law, we obtain

$$x(s) = H_{xm}(s)C(s)k_g r(s) + G(s)\eta(s) - H_{xm}(s)C(s)\tilde{\eta}(s) + x_{in}(s) \tag{19}$$

Taking the difference between (6) and (19),

$$\begin{aligned} x_{\text{ref}}(s) - x(s) &= G(s)(\eta_{\text{ref}}(s) - \eta(s)) + H_{xm}(s)C(s)\tilde{\eta}(s) \\ x_{\text{ref}}(s) - x(s) &= G(s)(\eta_{\text{ref}}(s) - \eta(s)) + H_{xm}(s)C(s)H_m^{-1}(s)C^\top \tilde{x}(s) \end{aligned} \tag{20}$$

Then, the following bound holds for $t \in [0, \tau]$:

$$\begin{aligned} \|x_{\text{ref}}(s) - x(s)\|_{\mathcal{L}_\infty} \leq \|G(s)\|_{\mathcal{L}_1} \|\eta_{\text{ref}}(s) - \eta(s)\|_{\mathcal{L}_\infty} \\ + \|H_{xm}(s)C(s)H_m^{-1}(s)C^\top\|_{\mathcal{L}_1} \|\tilde{x}_\tau(s)\|_{\mathcal{L}_\infty} \end{aligned} \tag{21}$$

From Assumption 1, it follows that

$$\begin{aligned} \|x_{\text{ref}}(s) - x(s)\|_{\mathcal{L}_\infty} \leq \|G(s)\|_{\mathcal{L}_1} L \|x_{\text{ref}}(s) - x(s)\|_{\mathcal{L}_\infty} \\ + \|H_{xm}(s)C(s)H_m^{-1}(s)C^\top\|_{\mathcal{L}_1} \gamma_0 \end{aligned} \tag{22}$$

which leads to the bound

$$\|x_{\text{ref}}(s) - x(s)\|_{\mathcal{L}_\infty} \leq \frac{\|H_{xm}(s)C(s)H_m^{-1}(s)C^\top\|_{\mathcal{L}_1}}{1 - \|G(s)\|_{\mathcal{L}_1} L}\gamma_0 \tag{23}$$

Now, taking the difference between the reference system and plant control inputs,

$$\begin{aligned} u_{\text{ref}}(s) - u(s) = -\frac{C(s)}{\omega}(\phi(s)\eta_{\text{ref}}(s) - k_g r(s)) \\ + \frac{C(s)}{\omega}(\phi(s)\eta(s) + \tilde{\eta}(s) - k_g r(s)) \end{aligned} \tag{24}$$

Hence,

$$u_{\text{ref}}(s) - u(s) = -\frac{C(s)}{\omega}\phi(s)(\eta_{\text{ref}}(s) - \eta(s)) + \frac{C(s)}{\omega}\tilde{\eta}(s) \tag{25}$$

and the following bound holds for $t \in [0, \tau]$:

$$\begin{aligned} \|u_{\text{ref}}(s) - u(s)\|_{\mathcal{L}_\infty} \leq \left\| \frac{C(s)}{\omega}\phi(s) \right\|_{\mathcal{L}_1} L \|x_{\text{ref}}(s) - x(s)\|_{\mathcal{L}_\infty} \\ + \left\| \frac{C(s)H_m^{-1}(s)C^\top}{\omega} \right\|_{\mathcal{L}_1} \|\tilde{x}_\tau(s)\|_{\mathcal{L}_\infty} \end{aligned} \tag{26}$$

which leads to the bound on the input,

$$\|u_{\text{ref}}(s) - u(s)\|_{\mathcal{L}_\infty} \leq \left\| \frac{C(s)}{\omega} \phi(s) \right\|_{\mathcal{L}_1} L\gamma_1 + \left\| \frac{C(s)H_m^{-1}(s)C^\top}{\omega} \right\|_{\mathcal{L}_1} \gamma_0 \tag{27}$$

□

## 4. Simulation Results

In this section, simulation results of the proposed output feedback proportional $\mathcal{L}_1$ adaptive controller are presented. The proportional $\mathcal{L}_1$ adaptive controller is compared with both a PID controller and the piecewise adaptation output feedback controller presented in [15]. The piecewise controller design is detailed in Appendix A.

The dynamics of the aerofoil can be represented by a second-order differential equation:

$$I\ddot{\alpha}(t) = -\bar{q}Sl_0a_1\alpha(t) + \bar{q}S(l_0a_2 + cm_0)\delta(t) - b\dot{\alpha}(t) \tag{28}$$

where $i$ is the moment of inertia of the aerofoil; $\alpha$ is the angle of attack, also equal to the pitch angle; $\bar{q}$ is the dynamic pressure; $S$ is the wing area; $l_0$ is the length between aerodynamic centre and pivot point; $c$ is the chord length; $a_1$, $a_2$, $m_0$, $b$ are aerodynamic derivatives; and $\delta$ is the elevator deflection angle, as illustrated in Figure 3.

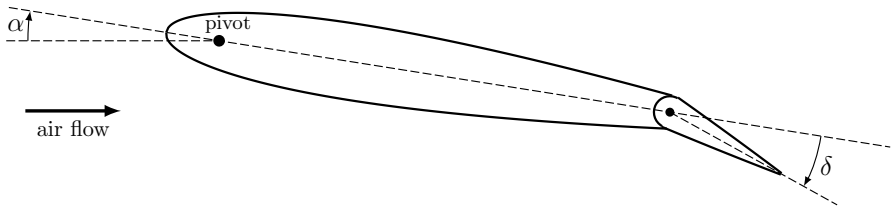


**Figure 3.** Aerofoil showing pitch and elevator deflections.

Equation (28) is linear for angles of attack below stall, so a Laplace transfer function representation could be obtained by determining the coefficient values in the differential equation. However, Duran [30] used second-order identification techniques to model the aerofoil as

$$\alpha(s) = \frac{44.94}{s^2 + 5.12s + 89.87}\delta(s) \tag{29}$$

The initial step in the process was to design a PID controller with two degrees of freedom, allowing for separate weightings to be adjusted for both the proportional and derivative terms. This specific controller, in parallel form, is expressed by

$$K(s) = K_p(b\alpha_{ref} - \alpha) + K_i\frac{(\alpha_{ref} - \alpha)}{s} + K_d\frac{N}{1 + N/s}(c\alpha_{ref} - \alpha) \tag{30}$$

where $\alpha_{ref}$ is the output reference angle; $K_i$, $K_p$ and $K_d$ are the integral, proportional and derivative gain, respectively; $N$ is the filter coefficient; and $b$ and $c$ are weightings for the proportional and derivative terms, respectively, that assign the closed-loop system zeros.

The PID parameters were tuned to achieve the desired performance with values $K_p = 0.435$, $K_i = 4.427$, $K_d = 0.0395$, $N = 52.68$, $b = 1$ and $c = 0$.

Figure 4 depicts the obtained system response for the PID controller. Similarly, the system response is displayed for both the adaptive controllers in Figure 5. All the responses exhibit zero overshoot, accompanied by a short rise time. Moreover, the control signals display smooth variation, devoid of any noise components. This characteristic ensures the prevention of any potential actuator damage.

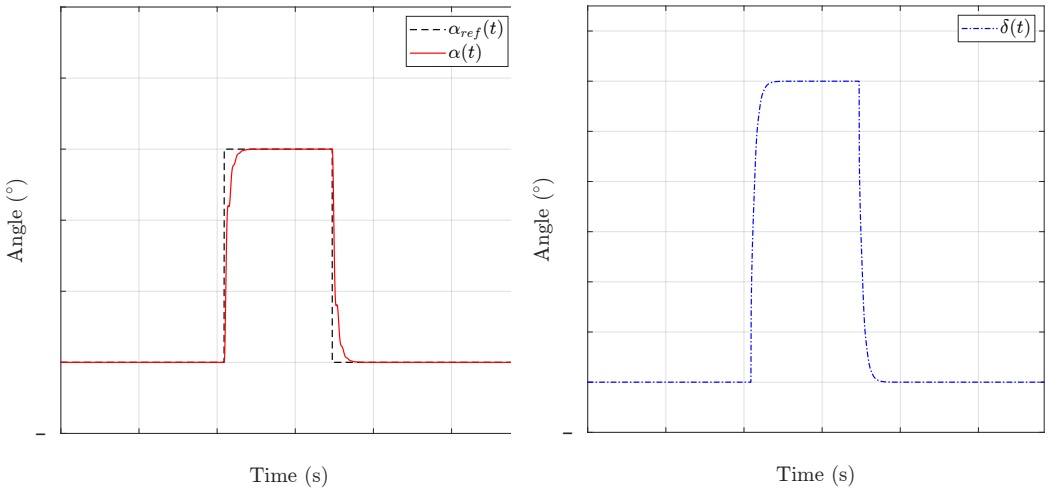


(**a**) System response. (**b**) Control history.

**Figure 4.** PID control simulation response.

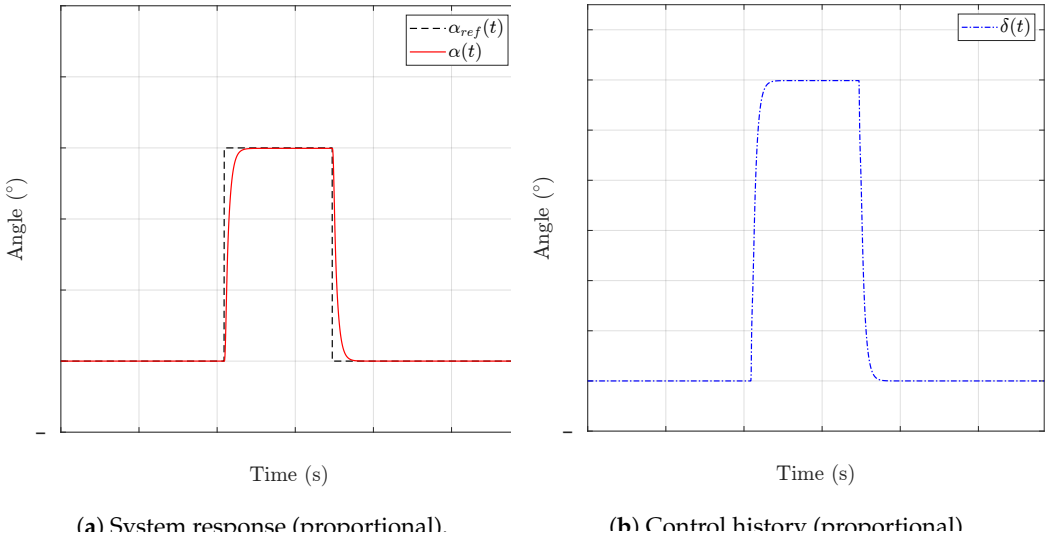


(**a**) System response (proportional). (**b**) Control history (proportional)

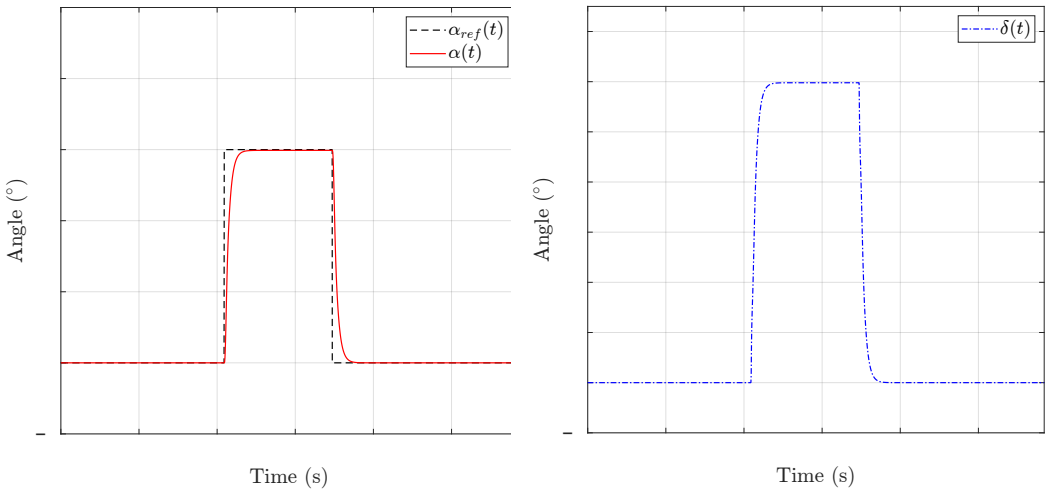


(**c**) System response (piecewise). (**d**) Control history (piecewise).

**Figure 5.** $\mathcal{L}_1$ adaptive control simulation response.

## 5. Implementation Results

The implementation of the proportional and the piecewise $\mathcal{L}_1$ adaptive controllers on the flight demonstrator unit are presented in this section. All the controllers are implemented using the Arduino IDE [34] in the C++ programming language. The PID algorithm was previously coded by [31] and is now utilised to obtain real-time responses by incorporating the PID parameters from the simulation.

In this $\mathcal{L}_1$ adaptive controller implementation, the desired model was chosen to achieve second-order dynamics with a frequency of 0.7: rad/s and a damping ratio of 0.7. The transfer function $D(s)$ of the $\mathcal{L}1$ adaptive controller was set as $D(s) = 1/s(s + 9.8)$, and $k = 36$, resulting in a filter $C(s) = 36/s^2 + 9.6s + 36$. The adaptation rate of the proportional controller was set at $\Gamma = 1000$, given that the sampling time of the test bed is $T_s = 0.0001$ s. This choice is based on the guideline that $\Gamma = 1/T_s$ [35].

### *5.1. Nominal Performance*

Figure 6a illustrates the response to a command angle of 6° using the PID parameters obtained from the simulation stage. The control history is also depicted in Figure 6b.

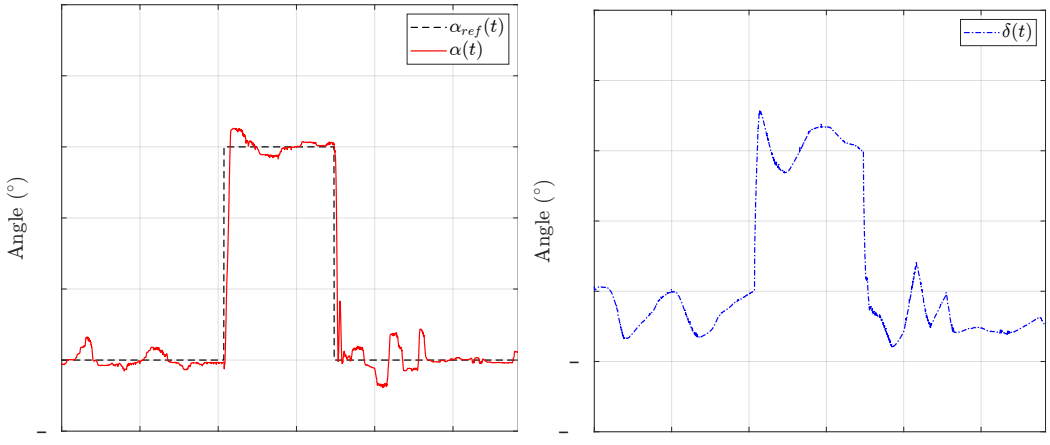


**(a)** System response. **(b)** Control history.

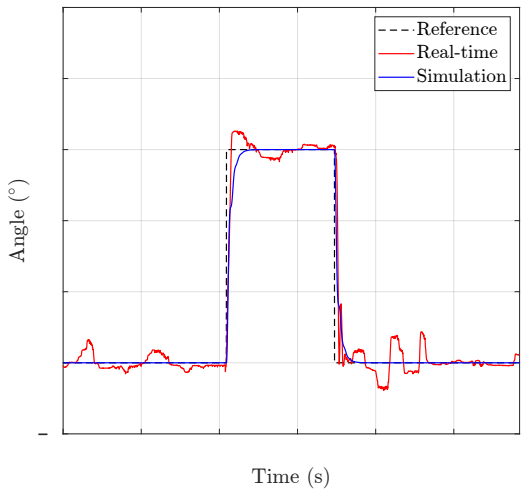


**(c)** System response comparison.

**Figure 6.** Real-time response with PID control.

The results are good, with overshoot being 8.67% and no steady-state error observed in the system. Moreover, the system effectively rejects disturbances, and the response is satisfactory, characterised by smooth variations in the control signal. Comparing the real-time response to the simulation depicted in Figure 6c, it is evident that the real-time system shows higher overshoot and more pronounced oscillations. However, it demonstrates a faster response with a rise time of 0.51 s, in contrast to the simulation rise time of 0.92 s. The disturbances are mostly in the airflow; the wind tunnel has not been specifically designed to create a smooth, steady laminar flow so that the disturbance rejection properties of the controller can be tested.

Likewise, Figure 7a illustrates the response of the proportional adaptive law. The control design demonstrates a good response in the form of a minimal overshoot of 6%. In comparison to the PID control history, the proportional adaptive law response appears noisier, which could be attributed to the utilisation of a larger bandwidth for the low-pass filter. However, it boasts a faster rise time of 0.64 s, outperforming the simulated rise time of 1 s.

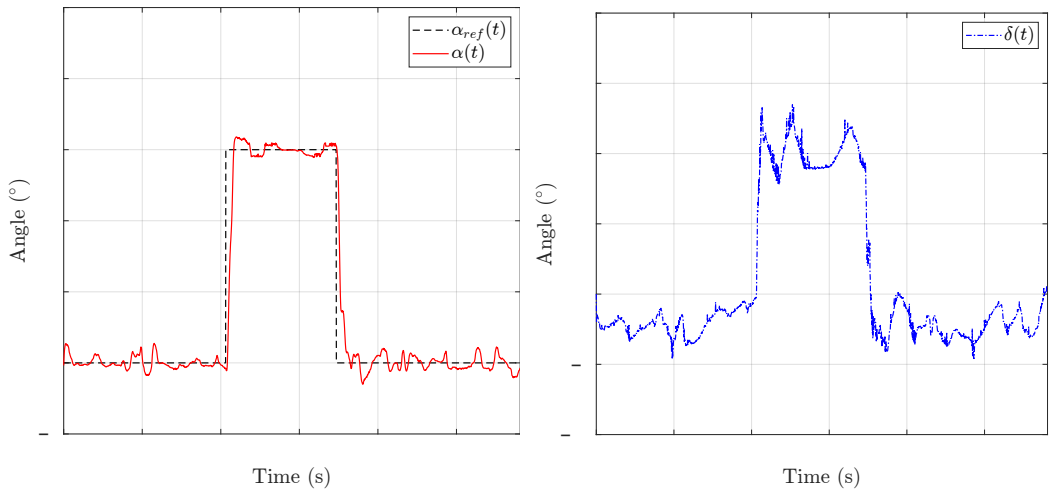


(**a**) System response. (**b**) Control history.

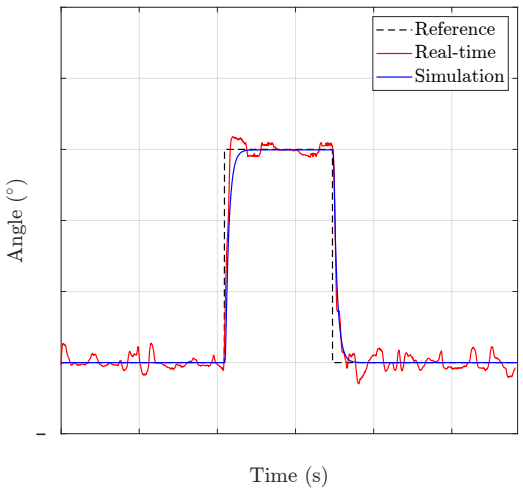


(**c**) System response comparison.

**Figure 7.** Real-time response with $\mathcal{L}_1$ adaptive control (proportional).

Lastly, Figure 8 presents the results of the piecewise algorithm. Among all the controller designs, it demonstrates the most favourable performance with the lowest overshoot of 3.17%. Additionally, it achieves a rapid rise time of 0.56 s. However, like the proportional

law, the control signal is quite noisy in comparison to the smoother control signal observed in the PID controller. Note that when the reference is zero, greater oscillation is evident. The NACA0012 aerofoil is relatively thick; hence, at low Reynolds numbers (as in this experiment), there is a nonlinearity in the control surface effectiveness, which results from flow separation that occurs on both the upper and lower surfaces and from the formation of a laminar separation bubble [36]. This also causes a reduction in the elevator effectiveness at low angles of attack.

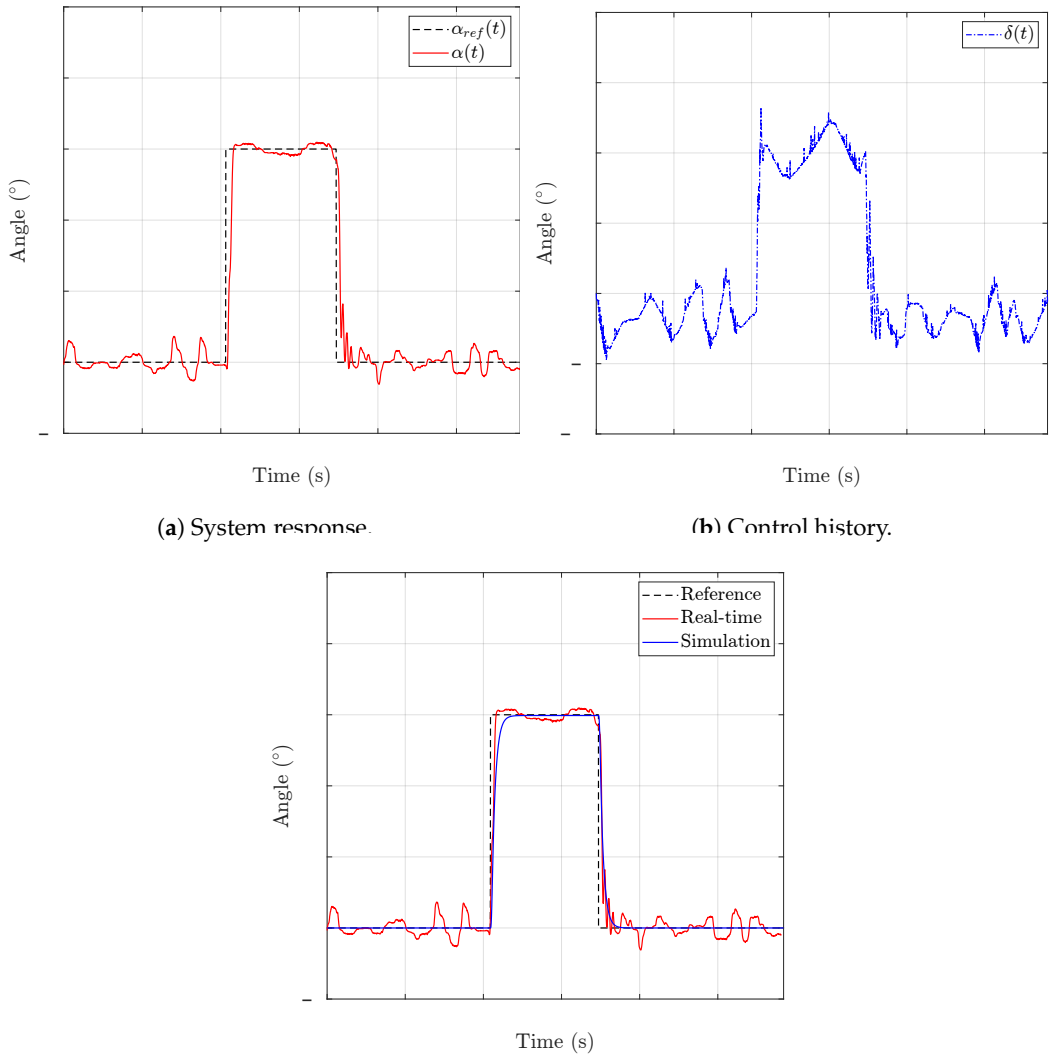


**(a)** System response. **(b)** Control history.

**(c)** System response comparison.

**Figure 8.** Real-time response with $\mathcal{L}_1$ adaptive control (piecewise).

### *5.2. Robustness Analysis*

The key advantage of $\mathcal{L}_1$ adaptive control lies in its robustness without compromising the adaptation gain. To demonstrate the robustness, various types of disturbances were introduced in the control channel at around 25 s.

In the first test, the control effectiveness is decreased by thirty percent. The PID Control response decreases to approximately 3.24°, whereas both adaptive controller responses drop to 4.64°, before eventually recovering to the reference command. This behaviour is illustrated in Figure 9a, where it is clear that both adaptive control designs outperform the PID control, exhibiting better performance despite the reduction in control effectiveness. The adaptive controllers adapt more effectively to the changes in the system and maintain better control throughout the process. Figure 9b shows that the reduced

control effectiveness leads to an increased control effort requirement for compensation. This heightened control effort is sustained until the end of the operation.

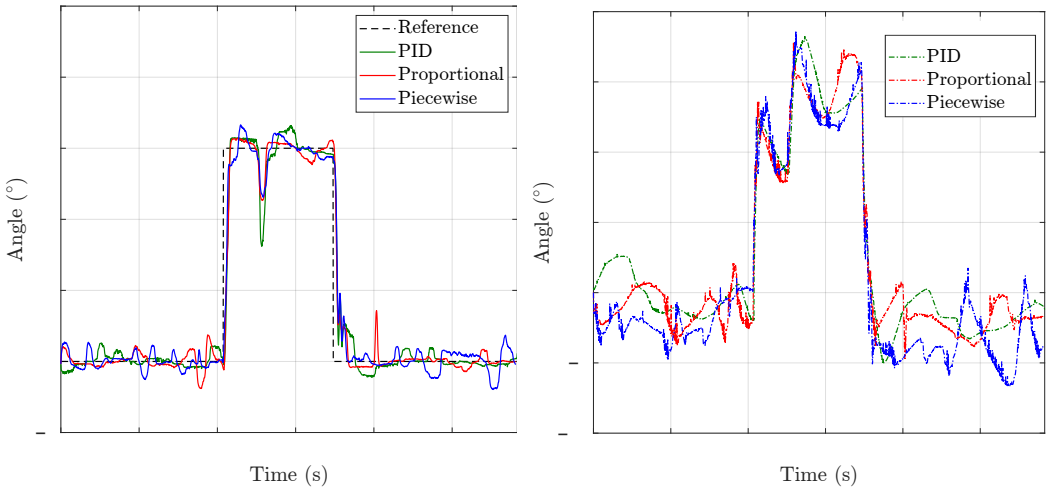


(**a**) System response. (**b**) Control history.

**Figure 9.** System response with reduced control effectiveness.

In the second comparison, a time-varying disturbance is introduced into the control channel, in the form of a sine wave with a frequency of 10 rad/s. The response of the control system is analysed, and the results are shown in Figure 10a. It can be observed that with PID control, the system experiences a sudden overshoot due to the disturbance. However, both adaptive control designs handle the time-varying disturbance effectively, as they do not exhibit significant overshoot. The compensation effects are depicted in Figure 10b, where the control signal of the adaptive designs shows the development of high-frequency content. This indicates that the adaptive controllers are actively adjusting to the changing disturbance and effectively maintaining control over the system.

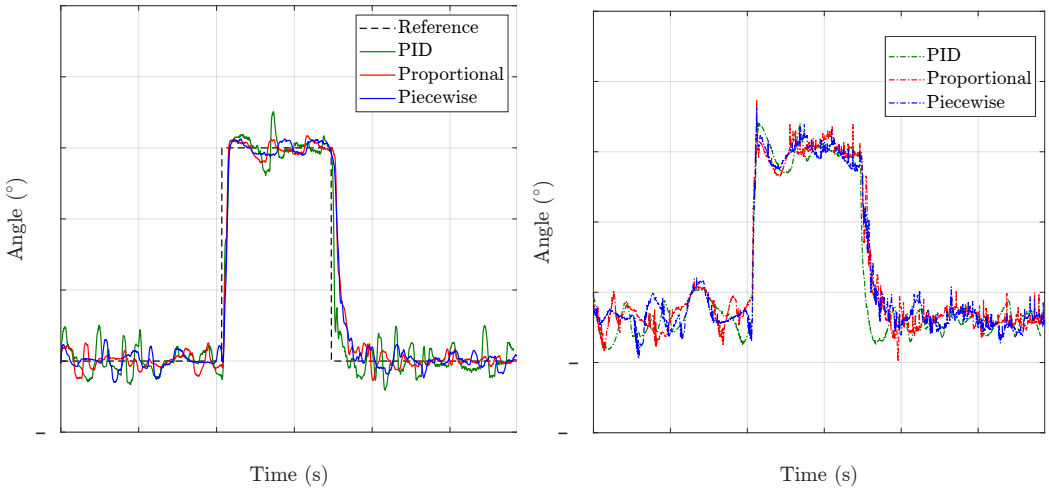


(**a**) System response. (**b**) Control history.

**Figure 10.** System response with time varying disturbance.

Another robustness check is conducted by introducing a 2° bias in the control channel. Interestingly, there is no significant difference in the response when this bias is introduced for all the controllers. However, when the reference is set back to zero, large oscillations

are observed, as shown in Figure 11a. Figure 11b shows the control history, revealing a constant offset in the control signal intended to compensate for the introduced bias.

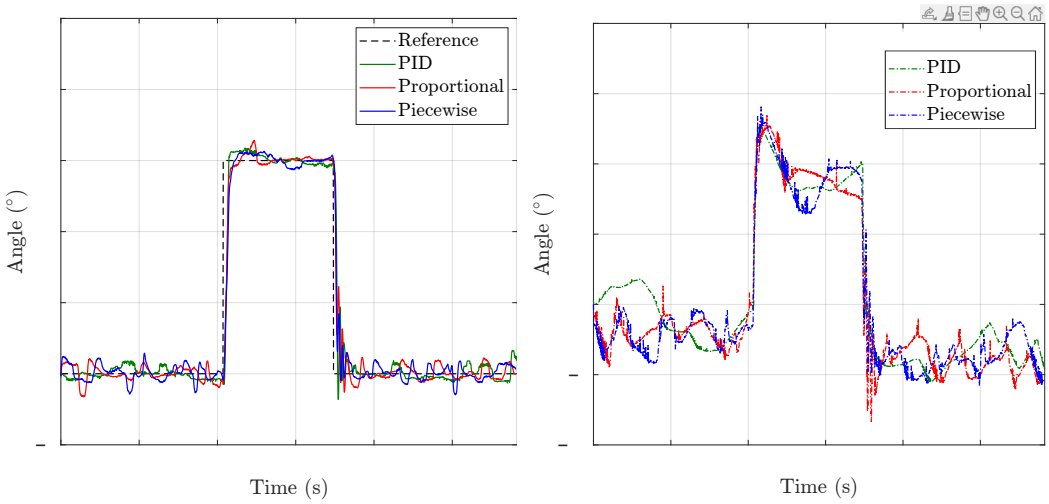


(**a**) System response. (**b**) Control history.

**Figure 11.** System response with bias.

To further evaluate the robustness of the control systems, different forms of disturbances are combined. The first combination includes a thirty percent reduction in control effectiveness along with a time-varying disturbance represented as a sine wave with a frequency of 10 rad/s. The results, as shown in Figure 12a, indicate that the PID control performs poorly in handling the time-varying disturbance compared to both adaptive controllers. On the other hand, the $\mathcal{L}_1$ adaptive control demonstrates effective compensation for both types of disturbances, as depicted in Figure 12b. However, after the introduction of the disturbances, the control signal becomes noisier and exhibits a simultaneous increase in control effort.

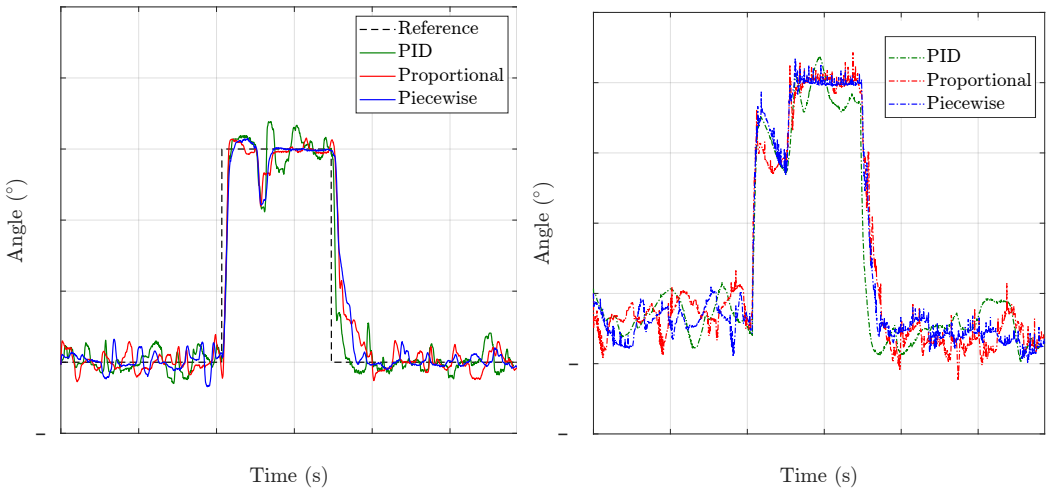


(**a**) System response. (**b**) Control history.

**Figure 12.** System response with reduced control effectiveness and time varying disturbance.

The impact of introducing a two-degree bias and thirty percent control reduction can be observed in Figure 13. Like the scenario with only control reduction, the PID response shows a lower performance compared to both adaptive controllers. Conversely, both adaptive controllers handle the combined disturbances effectively, resulting in better control

responses. The control history of the adaptive controllers demonstrates the necessary variations required to compensate for the reference command appropriately, ensuring a more robust and stable control performance.

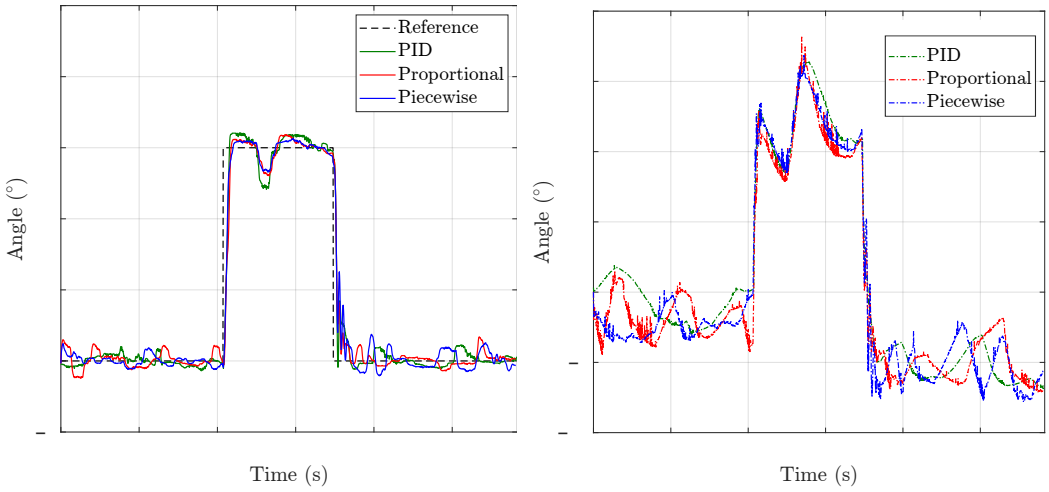


(**a**) System response. (**b**) Control history.

**Figure 13.** System response with bias and reduced control effectiveness.

## 6. Conclusions

An output feedback $\mathcal{L}_1$ adaptive control approach employing a proportional adaptation law is introduced. This method enhances the phase margin within the estimation loop, facilitating the integration of first-order sensor dynamics into the state predictor. Moreover, the reduction in error bounds is directly proportional to the adaptation gain, rather than its square root, leading to decreased computational resource requirements.

The design was implemented and tested on a benchtop flight control demonstrator, that being an airfoil pitch control system. To evaluate its robustness, different types of disturbances were introduced. The results demonstrate that the proposed method, along with the piecewise adaptive controller, outperforms PID Control when dealing with reduced control effectiveness and time-varying disturbances.

In $\mathcal{L}_1$ adaptive control, a key challenge lies in selecting the appropriate structure and parameters for the low-pass filter, especially in output feedback designs. Currently, no established principles guide this selection, leading to a trial-and-error approach in choosing the filter structure. This results in an ongoing challenge to achieve an optimal filter structure that balances performance and robustness effectively.

The implications of the nonlinearities of the control surface effectiveness on the control system performance remains to be fully analysed. An accurate model of the aerodynamics requires experiment in a high quality wind tunnel. The effect of the nonlinearities on the closed loop performance could then be analysed and simulated. This remains for further work.

**Author Contributions:** Conceptualisation, T.S. and J.F.W.; methodology, T.S.; software, D.B.; validation, D.B.; formal analysis, D.B. and T.S.; investigation, D.B.; resources, J.F.W.; data curation, D.B.; writing—original draft preparation, D.B.; writing—review and editing, T.S. and J.F.W.; visualisation, D.B. and J.F.W.; supervision, T.S. All authors have read and agreed to the published version of the manuscript.

**Funding:** This research received no external funding.

**Data Availability Statement:** TBD.

**Conflicts of Interest:** The authors declare no conflicts of interest.

## Appendix A

*Appendix A.1. $\mathcal{L}_1$ Piecewise Adaptive Law*

The plant dynamics are represented in slightly different state space form:

$$\begin{aligned} \dot{x}(t) &= A_m x(t) + B_m(u(t) + \sigma(t)) \\ y(t) &= C^\top x(t), \;\; x(0) = x_0 = 0, \end{aligned} \tag{A1}$$

where $\sigma(t)$ is the overall uncertainties arising from plant dynamics and external disturbances.

**Assumption A1.** *The given control design assumes that there exists positive constants, denoted as L and B, such that*

$$\begin{aligned} &\|f(t, y_1) - f(t, y_2)\|_\infty \leq L\|y_1 - y_2\|_\infty \\ &\|f(t, y)\|_\infty \leq L\|y\|_\infty + B \end{aligned}$$

*where the numbers L and B can be arbitrarily large.*

The architecture of the piecewise adaptive control differs slightly from the proportional version in that it does not factor in the input gain as part of its consideration.

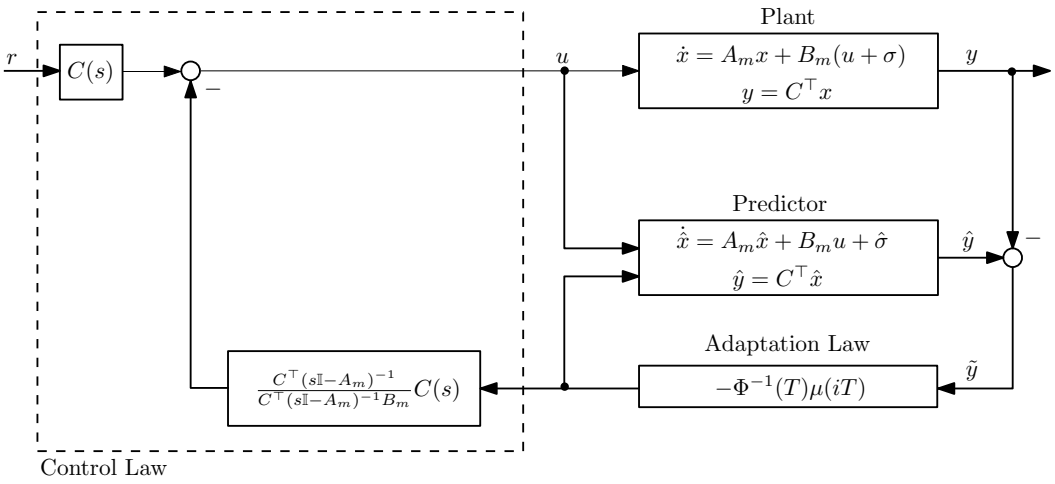


**Figure A1.** $\mathcal{L}_1$ adaptive control architecture (piecewise).

**State Predictor**: Consider the following state predictor,

$$\begin{aligned} \dot{\hat{x}}(t) &= A_m \hat{x}(t) + B_m u(t) + \hat{\sigma}(t), \;\; \hat{x}(0) = \hat{x}_0 = 0 \\ \hat{y}(t) &= C^\top \hat{x}(t) \end{aligned} \tag{A2}$$

Here, $\hat{\sigma}(t)$ is denoted to represent the overall vector of estimates.

**Adaptation Law**: There exists a $P = P^\top > 0$, which satisfies the following Lyapunov equation:

$$A_m^\top P + P A_m = -Q$$

where $Q > 0$, and given the properties of $P$, there exists a $D$, which represents the null space of $C^\top(\sqrt{P})^{-1}$, and letting

$$\Lambda = \begin{bmatrix} C^\top \\ D\sqrt{P} \end{bmatrix} \tag{A3}$$

Adaptation is governed by the following law:

$$\hat{\sigma}(iT) = -\Phi^{-1}(T)\mu(iT), \;\; i = 1, 2 \ldots \tag{A4}$$

where

$$\Phi(T) = \int_0^T e^{\Lambda A_m \Lambda^{-1}(T-\tau)} \Lambda d\tau \tag{A5}$$

and

$$\mu(iT) = e^{\Lambda A_m \Lambda^{-1} T} \mathbf{1}_1 \tilde{y}(iT), \;\; i = 1, 2 \ldots \tag{A6}$$

with $\mathbf{1}_1$ being a basis vector of length equal to number of states.

**Control Law**: The control law is defined through a low-pass filter represented by transfer function $C(s)$,

$$u(s) = C(s)\left(r(s) - \frac{C^\top (s\mathbb{I} - A_m)^{-1}}{C^\top (s\mathbb{I} - A_m)^{-1} B_m} \hat{\sigma}(s)\right) \tag{A7}$$

Furthermore, the selection of $C(s)$ and $M(s)$ must ensure that the following transfer function is stable:

$$H(s) = \frac{A(s)M(s)}{C(s)A(s) + (1 - C(s))M(s)}$$

and the given $\mathcal{L}_1$-norm condition should hold:

$$\|G(s)\|_{\mathcal{L}_1} L < 1$$

where $G(s) = H(s)(1 - C(s))$.

## References


1. Nelson, R.C. *Flight Stability and Automatic Control*; McGraw-Hill Education: New York, NY, USA, 2013.
2. Aström, K.J.; Wittenmark, B. *Adaptive Control*; Dover Publications: Mineola, NY, USA, 2010.
3. Shackcloth, B.; Butchart, R.L. Synthesis of model reference adaptive systems by Liapunov's second method. *IFAC Proc. Vol.* **1965**, *2*, 145–152. https://doi.org/10.1016/S1474-6670(17)69028-1.
4. Hovakimyan, N.; Cao, C. $\mathcal{L}_1$ *Adaptive Control Theory: Guaranteed Robustness with Fast Adaptation*; SIAM: Philadelphia, PA, USA, 2010. https://doi.org/10.1137/1.9780898719376.
5. Cao, C.; Hovakimyan, N. Design and analysis of a novel $\mathcal{L}_1$ adaptive control architecture with guaranteed transient performance. *IEEE Trans. Autom. Control* **2008**, *53*, 586–591. https://doi.org/10.1109/tac.2007.914282.
6. Gregory, I.; Cao, C.; Xargay, E.; Hovakimyan, N.; Zou, X. $\mathcal{L}_1$ adaptive control design for NASA AirSTAR flight test vehicle. In Proceedings of the AIAA Guidance, Navigation, and Control Conference, Chicago, IL, USA, 10–13 August 2009; p. 5738. https://doi.org/10.2514/6.2009-5738.
7. Xargay, E.; Dobrokhodov, V.; Kaminer, I.; Pascoal, A.M.; Hovakimyan, N.; Cao, C. Time-Critical Cooperative Control of Multiple Autonomous Vehicles: Robust Distributed Strategies for Path-Following Control and Time-Coordination over Dynamic Communications Networks. *IEEE Control Syst. Mag.* **2012**, *32*, 49–73. https://doi.org/10.1109/MCS.2012.2205477.
8. Dobrokhodov, V.; Xargay, E.; Hovakimyan, N.; Kaminer, I.; Cao, C.; Gregory, I.M. Multicriteria analysis of an $\mathcal{L}_1$ adaptive flight control system. *Proc. Inst. Mech. Eng. Part I J. Syst. Control Eng.* **2013**, *227*, 413–427. https://doi.org/10.1177/0959651812468545.
9. Cichella, V.; Kaminer, I.; Dobrokhodov, V.; Xargay, E.; Choe, R.; Hovakimyan, N.; Aguiar, A.P.; Pascoal, A.M. Cooperative path following of multiple multirotors over time-varying networks. *IEEE Trans. Autom. Sci. Eng.* **2015**, *12*, 945–957. https://doi.org/10.1109/TASE.2015.2406758.
10. Suárez Fernández, R.A.; Dominguez, S.; Campoy, P. $\mathcal{L}_1$ adaptive control for wind gust rejection in quad-rotor UAV wind turbine inspection. In Proceedings of the 2017 International Conference on Unmanned Aircraft Systems (ICUAS), Miami, FL, USA, 13–16 June 2017; pp. 1840–1849. https://doi.org/10.1109/ICUAS.2017.7991485.
11. Xu, D.; Whidborne, J.F.; Cooke, A. Fault tolerant control of a quadrotor using $\mathcal{L}_1$ adaptive control. *Int. J. Intell. Unmanned Syst.* **2016**, *4*, 43–66. https://doi.org/10.1108/IJIUS-08-2015-0011.
12. Ackerman, K.A.; Xargay, E.; Choe, R.; Hovakimyan, N.; Cotting, M.C.; Jeffrey, R.B.; Blackstun, M.P.; Fulkerson, T.P.; Lau, T.R.; Stephens, S.S. Evaluation of an $\mathcal{L}_1$ adaptive flight control law on Calspan's variable-stability Learjet. *J. Guid. Control Dyn.* **2017**, *40*, 1051–1060. https://doi.org/10.2514/1.G001730.
13. Zhou, Y.; Liu, H.; Guo, H.; Duan, X. $\mathcal{L}_1$ adaptive dynamic inversion attitude control for unmanned aerial vehicle with actuator failures. *Proc. Inst. Mech. Eng. Part G J. Aerosp. Eng.* **2019**, *233*, 4129–4140. https://doi.org/10.1177/0954410018814602.
14. Cao, C.; Hovakimyan, N. $\mathcal{L}_1$ adaptive output feedback controller for systems of unknown dimension. *IEEE Trans. Autom. Control* **2008**, *53*, 815–821. https://doi.org/10.1109/acc.2007.4282999.

15. Cao, C.; Hovakimyan, N. $\mathcal{L}_1$ adaptive output feedback controller for non strictly positive real reference systems with applications to aerospace examples. In Proceedings of the AIAA Guidance, Navigation and Control Conference and Exhibit, Honolulu, HI, USA, 18–21 August 2008; p. 7288. https://doi.org/10.2514/1.40877.
16. Mahdianfar, H.; Hovakimyan, N.; Pavlov, A.; Aamo, O.M. $\mathcal{L}_1$ adaptive output regulator design with application to managed pressure drilling. *J. Process Control.* **2016**, *42*, 1–13. https://doi.org/10.1016/j.jprocont.2016.02.004.
17. Lee, H.; Snyder, S.; Hovakimyan, N. $\mathcal{L}_1$ adaptive output feedback augmentation for missile systems. *IEEE Trans. Aerosp. Electron. Syst.* **2017**, *54*, 680–692. https://doi.org/10.1109/TAES.2017.2764218.
18. Zhu, R.; Yin, G.; Chen, Z.; Zhang, S.; Guo, Z. Temperature control of cryogenic wind tunnel with a modified $\mathcal{L}_1$ adaptive output feedback control. *Meas. Control* **2018**, *51*, 498–513. https://doi.org/10.1177/0020294018808672.
19. Ma, T.; Cao, C. $\mathcal{L}_1$ adaptive output-feedback control of multivariable nonlinear systems subject to constraints using online optimization. *Int. J. Robust Nonlinear Control* **2019**, *29*, 4116–4134. https://doi.org/10.1002/rnc.4597.
20. Ma, T.; Cao, C. $\mathcal{L}_1$ adaptive control for general partial differential equation (PDE) systems. *Int. J. Gen. Syst.* **2019**, *48*, 656–689. https://doi.org/10.1080/03081079.2019.1609955.
21. Zhou, Y.; Liu, H.; Guo, H. $\mathcal{L}_1$ adaptive output-feedback fault-tolerant control for uncertain nonlinear systems subject to unmodeled actuator dynamics and faults. *Trans. Inst. Meas. Control* **2022**, *44*, 2177–2192. https://doi.org/10.1177/01423312221075470.
22. Souanef, T.; Fichter, W. Adaptive altitude hold of a small UAV with switching adaptation laws. *IFAC Proc. Vol.* **2013**, *46*, 212–217. https://doi.org/10.3182/20130902-5-DE-2040.00099.
23. Souanef, T. *Adaptive Guidance and Control of Small Unmanned Aerial Vehicles*; Shaker Verlag: Herzogenrath, Germany, 2019.
24. Souanef, T. $\mathcal{L}_1$ adaptive output feedback control of small unmanned aerial vehicles. *Unmanned Syst.* **2023**, *11*, 249–260. https://doi.org/10.1142/S2301385023500103.
25. Mansor, H.; Mohd-Noor, S.B.; Gunawan, T.S.; Khan, S.; Othman, N.I.; Tazali, N.; Islam, R.B. Performance comparisons between PID and adaptive PID controllers for travel angle control of a bench-top helicopter. *Int. J. Electr. Inf. Eng.* **2015**, *9*, 35–40. https://doi.org/10.5281/zenodo.1338022.
26. Quanser. *3 DOF Helicopter*; Product Info Sheet; Quanser: Markham, ON, Canada, 2015.
27. Subramanian, R.G.; Elumalai, V.K. Robust MRAC augmented baseline LQR for tracking control of 2 DoF helicopter. *Robot. Auton. Syst.* **2016**, *86*, 70–77. https://doi.org/10.1016/j.robot.2016.08.004.
28. Quanser. *2 DOF Helicopter*; Product Info Sheet; Quanser: Markham, ON, Canada, 2015.
29. Villarreal-Valderrama, F.; Takano De La Cruz, L.; Alvarez, U.; Amezquita-Brooks, L.; Liceaga-Castro, E. Design of an aircraft pitch control experimental test bench. In Proceedings of the IEEE International Autumn Meeting on Power, Electronics and Computing (ROPEC), Ixtapa, Mexico, 14–16 November 2018; pp. 1–6. https://doi.org/10.1109/ropec.2018.8661430.
30. Duran, J.R. Flight Desk Control Demonstrator. Master's Dissertation, Cranfield University, Bedfordshire, UK, 2018. https://doi.org/10.17862/cranfield.rd.8052650.
31. Duran, J.R.; Whidborne, J.F.; Carrizales, M.; Pontillo, A. A benchtop flight control demonstrator. *Int. J. Mech. Eng. Educ.* **2021**, *49*, 80–97. https://doi.org/10.1177/0306419019852688.
32. Vanness, J.; Kharisov, E.; Hovakimyan, N. $\mathcal{L}_1$ adaptive control with proportional adaptation law. In Proceedings of the American Control Conference (ACC), Montreal, QC, Canada, 27–29 June 2012; pp. 1919–1924. https://doi.org/10.1109/acc.2012.6315660.
33. Vanness, J. Two New Extensions to L1 Adaptive Control Theory. Ph.D. Thesis, University of Illinois at Urbana-Champaign, Champaign, IL, USA, 2012.
34. Arduino. Arduino—Home. 2024. Available online: http://www.arduino.cc (accessed on 15 September 2023).
35. Dobrokhodov, V.; Kaminer, I.; Kitsios, I.; Xargay, E.; Hovakimyan, N.; Cao, C.; Gregory, I.M.; Valavani, L. Experimental validation of $\mathcal{L}_1$ adaptive control: The Rohrs counterexample in flight. *J. Guid. Control Dyn.* **2011**, *34*, 1311–1328. https://doi.org/doi.org/10.2514/1.50683.
36. Anyoji, M.; Okamoto, M.; Hidaka, H.; Kondo, K.; Oyama, A.; Nagai, H.; Fujii, K. Control surface effectiveness of low Reynolds number flight vehicles. *J. Fluid Sci. Technol.* **2014**, *9*, JFST0072. https://doi.org/10.1299/jfst.2014jfst0072.

2024-05-02

# Design and implementation of an L1 adaptive proportional output feedback controller

Bagati, Deepanshu

MDPI

Bagati D, Souanef T, Whidborne JF. (2024) Design and implementation of an L1 adaptive proportional output feedback controller. Actuators, Volume 13, Issue 5, May 2024, Article number 172

https://doi.org/10.3390/act13050172